NMR studies of metallic tin confined within porous matrices

E. V. Charnaya,[1,2] Cheng Tien,[1] M. K. Lee,[1] and Yu. A. Kumzerov[3]
[1]*Department of Physics, National Cheng Kung University, Tainan, 70101 Taiwan*
[2]*Institute of Physics, St. Petersburg State University, St. Petersburg, Petrodvorets 198504, Russia*
[3]*A. F. Ioffe Physico-Technical Institute, RAS, St. Petersburg 194021, Russia*
(Received 23 November 2006; published 4 April 2007)

^{119}Sn NMR studies were carried out for metallic tin confined within synthetic opal and porous glass. Tin was embedded into nanoporous matrices in the melted state under pressure. The Knight shift for liquid confined tin was found to decrease with decreasing pore size. Correlations between NMR line shapes, Knight shift, and pore filling were observed. The melting and freezing phase transitions of tin under confinement were studied through temperature dependences of NMR signals upon warming and cooling. Melting of tin within the opal matrix agreed well with the liquid skin model suggested for small isolated particles. The influence of the pore filling on the melting process was shown.

DOI: 10.1103/PhysRevB.75.144101 PACS number(s): 68.65.−k, 76.60.−k, 61.82.Bg, 64.70.Dv

I. INTRODUCTION

Small metallic particles formed within nanoporous matrices provide good opportunity for studying size effects on various physical features of metals. Porous matrices filled with metals are also considered as promising composite materials for different technical applications. Their advantages consist in screening the confined particles from harmful environment and in fabricating particle arrays of known geometry, which is specified by the geometry of pore networks. Recently, great efforts were made to reveal the influence of nanoconfinement on properties of liquid and solid metals within porous matrices (see Refs. 1–7 and references therein). The alterations in the melting and freezing phase transitions, self-diffusion, superconductivity, and electronic structure were of particular interest and were probed with various experimental techniques. Nevertheless, despite the continuously increasing attention to such composite materials, the properties of many metals in confined geometry remained extremely poorly studied. A number of experiments were carried out on metals with low enough melting points, such as indium, gallium, or mercury, since they are easier to embed into pores under high pressure in the melted state. While tin is one of the often used metals in technical applications and has a rather low melting temperature, studies of tin in nanoporous matrices, to our knowledge, are limited to an observation of the superconductivity in tin within opals as reported in Ref. 8 and to Mössbauer spectroscopy of confined gray tin thin layers in Ref. 9.

NMR has proved to be an extremely powerful probe to study liquids, in particular, melted metals, in confined geometry. Because of high sensitivity to local structure, chemical bonding, and atomic mobility, NMR can give information about phase transitions, electronic properties, and diffusion processes. The information obtained by NMR can then be used to reveal size effects of different natures and to separate them from the influence of coupling of confined particles with the pore surface and between each other.

In the present paper, ^{119}Sn NMR was applied to studies of liquid metallic tin confined within porous matrices (synthetic opal and porous glass). Information about the melting and freezing phase transitions and electronic susceptibility in confined tin were obtained through observations of temperature dependences of the intensity of NMR signals upon warming and cooling and of alterations in the Knight shift and line shape.

II. EXPERIMENT

The NMR measurements of confined liquid metallic tin were carried out using a Bruker Avance 400 pulse spectrometer in a magnetic field of 9.4 T. Tin has three naturally occurring isotopes, in which the nuclei have nonzero magnetic moments. All three isotopes have spin $I=1/2$ and, thus, their quadrupole moment is equal to zero. Among them, the isotope ^{119}Sn shows the best NMR signals and was chosen for measurements in the present paper. Its natural abundance is 8.59%. The ^{119}Sn NMR line shape, intensity, and Knight shift were measured using a single pulse sequence with phase cycling within a temperature range from 515 K (above the bulk tin melting point of 505 K) down to the completely confined tin freezing temperature. The repetition time was 0.2 s. The rate of warming and cooling the samples under study was slow to prevent temperature overshoots, which did not exceed 0.3 K in our measurements. Below 410 K, temperature was changed slower than 1 K/min; within the range 410–515 K, the rate of cooling and melting was about 0.2 K/min. Prior to each measurement, the samples were kept at a fixed temperature for about 5 min. The NMR signals from ^{119}Sn were rather weak because of the low natural abundance of the isotope, so the necessary number of scans in our experiments varied from 4 000 to 40 000.

Two different porous matrices were used. The synthetic opal consisted of close packed silica spheres of 210 nm in diameter. Such an ideal structure should have octahedral and tetrahedral pores between adjacent spheres with radii $r_1=0.414R$ and $r_2=0.224R$, respectively (R is the radius of the constituent silica spheres). The number of tetrahedral pores is twice the number of octahedral ones. Mercury intrusion porosimetry (this method was described, for instance, in Ref. 10) for the opal sample under study revealed two kinds of pores as expected. Their radii lie in the range from

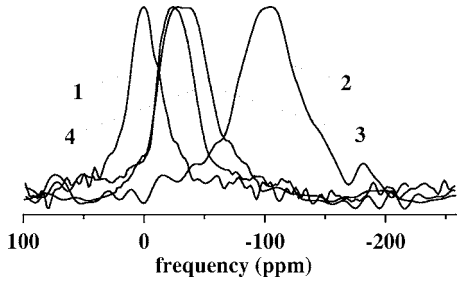

FIG. 1. ^{119}Sn NMR lines for bulk liquid tin (1) and liquid tin confined within porous glass (2) and opal with filling factors of 85% (3) and 40% (4). The lines for bulk and confined tin were obtained at 508 and 500 K, respectively.

28 to 35 nm with distinct distribution maximum at $r_1 = 30$ nm and in the range from 17 to 20 nm with distribution maximum at $r_2 = 18$ nm. The overall volume of these two kinds of pores was about 0.9 of the total pore volume, the total relative volumes of tetrahedral and octahedral pores being the same. The remaining pore volume was occupied by fine pores whose radius was less than 2 nm. The porous glass matrix was prepared from phase-separated soda borosilicate glass by acid leaching. The main pore radius, 4 nm, was also determined using mercury intrusion porosimetry. Pores with radii from 3.8 to 4.3 nm corresponded to 93% of the total pore volume. The rest of the pore volume was occupied by pores whose radii are less than 1 nm.

Liquid tin was embedded into the porous matrices under high pressure of up to 10 kbar. After the pressure was removed, some amount of tin flowed out of the pores. The filling factors evaluated by weighing the samples after cooling down to room temperature were 85% and 75% for the opal and glass, respectively. Since liquid tin, as mercury, does not wet the silica surface,[11] it gathers within bigger pores under the conditions of incomplete filling. Therefore, when the filling factor for the opal is 85%, almost all octahedral pores and a part of tetrahedral pores are filled with tin. According to the mercury porosimetry data mentioned above, the overall relative volume of filled octahedral pores is 0.45 and that of filled tetrahedral pores is 0.40. For the porous glass, all confined tin should be gathered within the 4 nm pores.

III. RESULTS

A. Knight shift in confined liquid tin

^{119}Sn NMR spectra for liquid tin within the opal and glass matrices are shown in Fig. 1 along with that for bulk melted tin. The spectrum for bulk melted tin was taken at 508 K just above the bulk melting point. The spectra for confined liquid tin were obtained at 500 K, when tin within pores was in the liquid state while tin on the sample surface (when it existed) was frozen. The Knight shifts for confined tin were referenced to the ^{119}Sn signal from bulk liquid tin. The spectra for liquid tin within the opal porous matrix shown in Fig. 1 were taken at two different filling factors. The broader line was obtained when the filling factor was 85%. Following successive warming-cooling cycles, the confined tin gradually

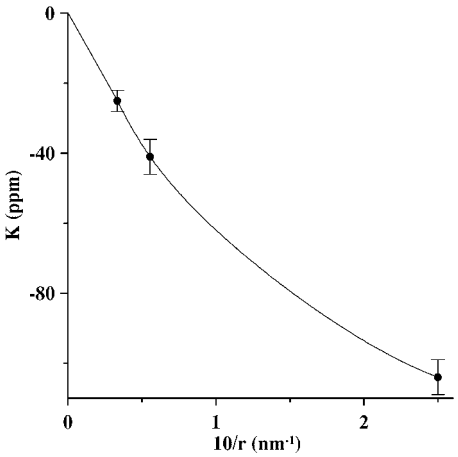

FIG. 2. Dependence of the Knight shift K relative to that in bulk liquid tin on the inverse pore radius r. The solid curve is a guide for the eyes.

flowed out of the pores, leading to a decrease of the filling factor. The second, narrower NMR line corresponding to the opal in Fig. 1 was taken when the filling was 40% of the total pore volume. At this filling, the liquid tin should mainly be gathered within octahedral pores of larger sizes. The ^{119}Sn NMR line for the porous glass did not change noticeably in shape and position upon decreasing the filling through repetitive warming, but its intensity gradually decreased.

Figure 1 shows that the ^{119}Sn NMR lines for liquid tin in porous matrices are shifted to low frequencies. The Knight shift for tin within the glass matrix decreased by 104 ± 5 ppm compared to that for bulk tin. The relative Knight shift for the opal at 40% filling is -25 ± 3 ppm. This shift obviously corresponds to tin within octahedral pores. Since the ^{119}Sn lines for the opal at less filling and for the porous glass with a single dominant size of filled pores show rather narrow tops contrary to the line for the opal at 85% filling, we treated the latter as an overlap of two lines caused by tin in octahedral and tetrahedral pores with relative Knight shifts of -25 ± 3 and -41 ± 5 ppm, respectively. Such attribution agrees with the bimodal distribution of filled pores at this filling factor (see also Sec. IV). The dependence of the ^{119}Sn Knight shift relative to its bulk value on the inverse pore radius is shown in Fig. 2.

Starting from about 503 K upon warming, one can see NMR signals from melted tin on the sample surfaces. Such signals appeared following three and more warming-cooling cycles after cleaning the sample surfaces for the opal sample and upon every warming for the glass sample. The signals from surface and confined tin are overlapped but can be easily resolved due to difference in the Knight shift. An example of the overlapped lines from surface and confined liquid tin in the opal sample is shown in Fig. 3. The position and the line shape of the ^{119}Sn NMR line from tin on the sample surface coincided with those from bulk tin within experimental accuracy (Fig. 3).

B. Melting and freezing of confined tin

The integral intensity of a ^{119}Sn NMR line is proportional to the total amount of liquid tin confined within pores at a

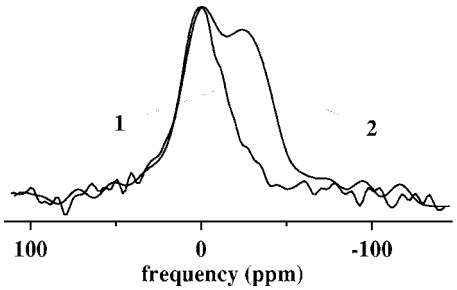

FIG. 3. ^{119}Sn NMR lines for bulk liquid tin (1) and for liquid tin confined within opal with filling factor of 40% and on the sample surface (2).

particular temperature. Therefore, the temperature dependence of the ^{119}Sn line integral intensity can be treated as a temperature dependence of the total amount of unfrozen confined tin. Figure 4 shows the variations of the ^{119}Sn line relative integral intensity upon warming and cooling the opal sample at 85% and 40% filling. Because of low signal-to-noise ratio and continuous losses in confined tin, it was impossible to obtain similar data for the porous glass. One can see in Fig. 4 that the confined tin melting process was remarkably broadened and shifted to low temperature compared to the bulk tin melting point. The melting onset and offset temperatures are about the same for both filling factors, but the amount of melted tin was quite different within the melting range. The freezing phase transition was also broadened and there was a pronounced hysteresis between the melting and freezing phase transitions. Liquid confined tin was found to be supercooled down to about 430 K.

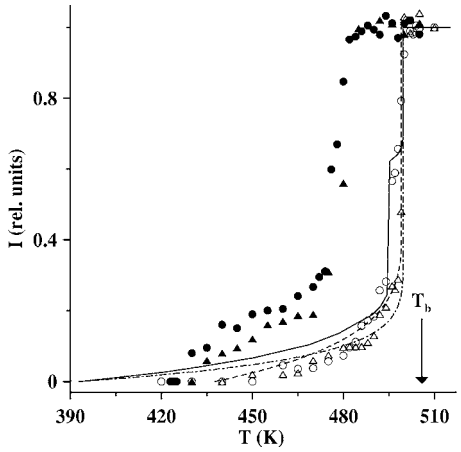

FIG. 4. Temperature dependence of the integral intensity I of the ^{119}Sn NMR line for liquid tin embedded in opal when the filling factors were 85% (circles) and 40% (triangles) upon warming (open symbols) and cooling (closed symbols). The solid and dash-dot lines show the theoretical dependences calculated with the liquid skin model using relationship (7) and the extrapolation length ξ=6 Å for the filling factors of 85% (solid line) and 40% (dash-dot line). The dashed line shows similar theoretical dependence for ξ=10 Å and 40% filling.

IV. DISCUSSION

A. Melting phase transition

Solid tin at temperatures higher than room temperature occurs as tetragonal metallic (white) β-tin. The density of β-modification near the melting point is 7.18 g/cm^3 and that of liquid tin just above the melting point is 6.98 g/cm^3.[12] Silica surface is nonwettable for liquid tin[11] (as for liquid mercury), the contact angle being larger than 110°. Since tin contracts upon freezing, we can suggest that after some amount of liquid tin flowed out of the porous matrices at high temperature during the preparation procedure the rest of the tin formed crystalline nanoparticles within pores through cooling, which are weakly linked to the inner matrix surface. Then the solid tin particle surface should be mostly free. This justifies the application to confined tin melting of theoretical models developed for melting of a single isolated small particle. The case of mostly nonwetting confined liquids is opposite in this regard to the case of wetting liquids.

Thermodynamic models of small particle melting predict a reduction of the melting temperature when the melt wets its own solid surface. The first idea of size effects on melting of small metallic particles was advanced by Pawlow.[13] He suggested that the melting point can be considered as a triple point, where the solid, melted, and vapor states are in equilibrium, and included in the thermodynamic potential the surface energy, which is important because of the increased surface to volume ratio in small particles. The decrease of the melting temperature ΔT for a spherical particle with radius R is then given by

$$\frac{\Delta T}{T_b} = \frac{2(\gamma_{sv} - \gamma_{lv})}{L\rho R}, \tag{1}$$

where $\Delta T = T_b - T_m$, T_b is the melting point of the relevant bulk, and T_m is the temperature of particle melting; γ_{sv} and γ_{lv} are the surface tensions for the solid-vapor and liquid-vapor boundaries, respectively; L is the latent heat of fusion; and ρ is the density. In Eq. (1), the difference between the density of liquid and solid was neglected. Often they use the Gibbs-Thompson equation to treat the melting temperature reduction in small particles,

$$\frac{\Delta T}{T_b} = \frac{2\gamma_{sl}}{L\rho R}, \tag{2}$$

where γ_{sl} is the surface tension at the boundary between the solid and its melt. Relationship (2) coincides with the low-exponent approximation of the relationship obtained in Ref. 14 for a particle within its own melt,

$$T_m = T_b \exp\left(-\frac{2\gamma_{sl}}{\rho L R}\right). \tag{3}$$

It was also suggested (see Ref. 15, for instance) to write the free-energy balance for the whole particle before and after the melting or freezing phase transition, which yields

$$\frac{\Delta T}{T_b} = \frac{3(\gamma_{sv} - \gamma_{lv})}{L\rho R}. \tag{4}$$

More complicated models account for the formation of a liquid skin on the surface of the solid core. First, such an idea was advanced in Refs. 16 and 17. The necessary condition for the thin surface layer melting is

$$\gamma_{sv} - \gamma_{sl} - \gamma_{lv} > 0. \tag{5}$$

Later it was shown[18] that the model predicts a stable liquid skin on the solid surface in a temperature range below the offset of melting only when one takes into account the influence of the solid core on the structure of the surface liquid layer.[19,20] Since the surface tension on the free surface of the liquid layer should approach γ_{sv} when the layer thickness $\delta \to 0$, the free energy of the liquid skin assumes the form

$$F_\delta = -N'\mu_s + N'\mu_l + 4\pi R^2\gamma_{lv} + 4\pi r^2\gamma_{sl} + (4\pi R^2\gamma_{sv} - 4\pi R^2\gamma_{lv} - 4\pi r^2\gamma_{sl})f(\delta), \tag{6}$$

where $f(\delta)=\exp(-\delta/\xi)$ for the metallic surface;[20] ξ is a parameter of the order of several angstroms, which can be named the extrapolation length. In Eq. (6), N' is the number of particles in the layer, r is the radius of the solid core, and μ_s and μ_l are chemical potentials of the solid and liquid, respectively. The free-energy extremum is achieved when

$$L\rho\frac{\Delta T}{T_b} = \frac{2\gamma_{sl}}{R-\delta}(1-e^{-\delta/\xi}) + \left[\gamma_{sv} - \gamma_{lv} - \frac{(R-\delta)^2}{R^2}\gamma_{sl}\right]\frac{R^2}{(R-\delta)^2}\frac{e^{-\delta/\xi}}{\xi}. \tag{7}$$

This relationship was obtained in Ref. 18. The extremum (7) corresponds to the equilibrium state with a solid core surrounded by the liquid skin when

$$-2\gamma_{sl}(1-e^{-\delta/\xi}) - 2(\gamma_{sv}-\gamma_{lv})\frac{R^2}{R-\delta}\frac{e^{-\delta/\xi}}{\xi} + \left[\gamma_{sv} - \gamma_{lv} - \frac{(R-\delta)^2}{R^2}\gamma_{sl}\right]R^2\frac{e^{-\delta/\xi}}{\xi^2} > 0. \tag{8}$$

According to relationships (7) and (8), the melted skin appears at a temperature corresponding to $\delta=0$,

$$L\rho\frac{\Delta T}{T_b} = (\gamma_{sv} - \gamma_{lv} - \gamma_{sl})\frac{1}{\xi}, \tag{9}$$

and achieves its maximal thickness with increasing temperature when the left part of the inequality (8) becomes zero. Then the solid core melts sharply.

Assuming that the surface of confined solid tin nanoparticles is mostly free and taking into account that condition (5) remains valid for tin,[21] we can apply the liquid skin model to treat the results obtained for the melting phase transition in tin embedded in opal (Fig. 4). The necessary parameters are $\gamma_{sv}=660$ mJ/m^2, $\gamma_{lv}=550$ mJ/m^2, $\gamma_{sl}=55$ mJ/m^2,[11,22,23] and $L=58.9$ J/g.[12] The extrapolation length ξ for tin was not obtained earlier from independent experiments. So, to treat the calorimetric studies of melting and freezing in unsupported tin cluster beams, Bachels *et al.*[21] used $\xi=6$ Å found previously for lead.[24] They obtained good agreement with their experiments, but also remarked that the agreement was better with some bigger extrapolation length, which could be explained by an increase in ξ upon increasing surface curvature.

We used $\xi=6$ Å to calculate the temperature dependence of the melted tin within the opal for two filling factors, corresponding to the results shown in Fig. 4. For 85% filling, the bimodal filled pore size distribution was taken into account, while for 40% filling, all the tin were assumed to be in octahedral pores. For both filling factors, the model predicts quite a large temperature range of coexistence of liquid skin and solid core for confined tin particles. Then at elevated temperatures, the melting should occur in two steps for the higher filling factor and in one step for the lower one. The solid core melting temperature reductions ΔT according to the liquid skin model are 9.9 and 5.4 K for tetrahedral and octahedral pores, respectively. The experiment and the model agree very well as can be seen in Fig. 4, except for the low-temperature tail; the model predicting the onset of melting at a much lower temperature than it was observed experimentally. Increasing ξ weakly influences the temperature of the melting offset while it noticeably improves the predictions of the model for the onset of melting as can be seen in Fig. 4, where the theoretical dependence of the relative amount of liquid tin through melting is shown by the dash line for $\xi=10$ Å and the 40% pore filling. Therefore, the melting of tin confined within the opal can be well described with the liquid skin model developed for small spherical particles. One can thus conclude that the melting phase transition in confined tin is mainly affected by size effects in nanoparticles rather than by the coupling between nanoparticles and with the pore surface. Note that melting of isolated and supported tin particles was also consistent with theoretical predictions for a small spherical particle,[21–23,25] while pronounced superheating was observed for α-tin thin films in Sn/Si multilayer structures.[9]

As was found also for other metallic and nonmetallic liquids in confined geometry, the freezing phase transition in tin embedded in opal was shifted to lower temperatures compared to the melting with pronounced thermal hysteresis, which is generally believed to be related to nucleation processes (see, for instance, Refs. 21 and 26).

B. Knight shift

The Knight shift in liquid metals like tin with closed inner electron subshells originates mainly from the Fermi contact interaction of the spin polarized conduction electrons with nuclei:[27–29]

$$K_s = \frac{8}{3}\pi\chi_s\Omega\langle|\Psi_F(0)|^2\rangle, \tag{10}$$

where χ_s is the electron spin susceptibility per unit volume, Ω is the atomic volume, and $\langle|\Psi_F(0)|^2\rangle$ is the probability density at the nucleus of s-like electrons on the Fermi surface. The contributions from the orbital hyperfine interaction and core polarization are small. Measurements on bulk liquid tin were consistent with theoretical examination and with spin-lattice relaxation studies.[28] According to Eq. (10), the Knight shift caused by the contact interaction is directly proportional to the electron spin susceptibility.

Until now, the influence of particle size reduction on the Knight shift was studied mostly for small isolated or supported metallic particles and thin layers in solid state (see Refs. 30–33 and references therein). At low temperatures, theories predict alterations in the Knight shift due to quantum size effects resulting from increasing conduction electron level separation (see Ref. 34 and references therein). However, at higher temperatures, the Knight shift could be affected chiefly by surface induced spatial variations in the density of electrons on the Fermi level which influence the total electron spin susceptibility because of increasing surface to volume ratio (see Ref. 35 and references therein). The surface induced effects in the spin susceptibility depend on the electron structure of the metals under study. For transition metals, the tight-binding approximation[35] predicts changes in the density of *d* electrons near the surface, which should lead to pronounced local shifts of NMR lines compared to bulk. The experimental results obtained for platinum and rhodium solid particles agree to a certain extent with this model.[32]

According to theoretical calculations carried out using the local density-functional formalism, the spin susceptibility for simple metals with closed inner electron subshells should show damped Friedel oscillations near the metal surface; the integral surface magnetic susceptibility increases compared to bulk.[35] This model was applied to treat the strong broadening of NMR lines due to the broad distribution in the Knight shift for small solid particles of metals such as Pb, Cu, or Ag.[32,36] The drastic resonance line broadening prevented clear observation of the size dependence of the Knight shift.

Contrary to the case of solid metals, the NMR lines for liquid nanoparticles should be narrowed due to atomic mobility. Thus, the Knight shift measured for confined liquid tin nanoparticles should correspond to whole particles and the decrease in the Knight shift observed in the present studies reflects the size dependence of averaged values of the shift. According to Eq. (10), one should expect that the enhancement predicted of the integral surface electron susceptibility could lead to a total increase in the Knight shift for liquid nanoparticles of nontransition metals. However, the observed shift of ^{119}Sn NMR lines to low frequencies for confined liquid tin contradicts these theoretical predictions.

A possible explanation of this discrepancy consists in the influence on the Knight shift in liquid tin of the core polarization effects. While the main contribution occurs due to contact hyperfine interaction with conduction electrons,[27–29] the surface induced alterations in core polarization effects might be more noticeable and thus control the size dependence of the Knight shift. Other possible explanations of the striking contrast between the experimental results and theory could arise from the influence on the electron properties of the interaction with the matrix inner surface. While this interaction was found not to be effective in melting, it may strongly influence the electronic surface properties of confined particles. Note that the Knight shift reduction with decreasing pore sizes was also observed in Ref. 37 for liquid gallium confined within porous glasses and opals.

The ^{119}Sn NMR lines in confined melted tin were almost as narrow as in the bulk (Fig. 1). Only the line for tin within the porous glass was somewhat broadened compared to the bulk. Since the spin of the ^{119}Sn isotope is 1/2, the NMR lines are not influenced by a conceivable slowdown of atomic self-diffusion under confinement similar to the confined mercury case[38] and in contrast to the remarkable NMR line broadening in liquid indium and gallium.[5,6] Therefore, the ^{119}Sn line shape in the samples under study is related to local magnetic field heterogeneities as in bulk liquid tin and, in addition, with heterogeneities in the Knight shift caused by the pore size distribution in the porous matrices. The latter agrees with the deconvolution of the ^{119}Sn line for the opal under 85% filling made in Sec. III A and resulting in two overlapped lines from tin confined within tetrahedral and octahedral pores.

In conclusion, ^{119}Sn NMR measurements of the line shape, Knight shift, and temperature dependence of the NMR signal intensity were carried out on metallic tin embedded in nanoporous matrices to study effects induced by confinement. The Knight shift in liquid tin showed a monotonic decrease with decreasing pore size in contrast with theoretical predictions for electronic susceptibility near the surface of metals with closed inner electron subshells. NMR line shape and shift were found to be sensitive to the filling factor of pores with tin due to the redistribution of tin over the pore volume. Both melting and freezing phase transitions in tin confined within the opal were broadened and shifted to low temperature with pronounced hysteresis upon warming and cooling. The general melting behavior depended on the filling factor, while the offset of melting and the overall temperature range of melting were almost identical. The liquid skin model of melting developed for isolated small metallic particles was shown to fit perfectly the melting process.

ACKNOWLEDGMENTS

The present work was supported by the Taiwan government under Grant No. OUA 95-21T-2-017 and by RFBR (Russia).

[1] A. Burchianti, A. Bogi, C. Marinelli, C. Maibohm, E. Mariotti, and L. Moi, Phys. Rev. Lett. **97**, 157404 (2006).

[2] Q. Xu, I. D. Sharp, C. W. Yuan, D. O. Yi, C. Y. Liao, A. M. Glaeser, A. M. Minor, J. W. Beeman, M. C. Ridgway, P. Kluth, J. W. Ager III, D. C. Chrzan, and E. E. Haller, Phys. Rev. Lett. **97**, 155701 (2006).

[3] C. B. Murray, C. R. Kagan, and M. G. Bawendi, Annu. Rev. Mater. Sci. **30**, 545 (2000).

[4] C. Tien, E. V. Charnaya, W. Wang, Yu. A. Kumzerov, and D. Michel, Phys. Rev. B **74**, 024116 (2006).

[5] E. V. Charnaya, C. Tien, Yu. A. Kumzerov, and A. V. Fokin, Phys. Rev. B **70**, 052201 (2004).

[6] E. V. Charnaya, T. Loeser, D. Michel, C. Tien, D. Yaskov, and Yu. A. Kumzerov, Phys. Rev. Lett. **88**, 097602 (2002).
[7] C. Tien, C. S. Wur, K. J. Lin, E. V. Charnaya, and Yu. A. Kumzerov, Phys. Rev. B **61**, 14833 (2000).
[8] V. N. Bogomolov, Y. A. Kumzerov, S. G. Romanov, and V. V. Zhuravlev, Physica C **208**, 371 (1993).
[9] B. R. Cuenya, W. Keune, W. A. Adeagbo, and P. Entel, Phys. Rev. B **73**, 045311 (2006).
[10] F. A. L. Dullien, *Porous Media: Fluid Transport and Pore Structure* (Academic, San Diego, 1992).
[11] A. Amirfazli, D. Chatain, and A. W. Neumann, Colloids Surf., A **142**, 183 (1998).
[12] *American Institute of Physics Handbook*, 3rd ed. (McGraw-Hill, New York, 1972).
[13] P. Pawlow, Z. Phys. Chem., Stoechiom. Verwandtschaftsl. **65**, 545 (1909).
[14] V. K. Semenchenko, *Surface Phenomena in Metals and Alloys* (Pergamon, New York, 1981), p. 281.
[15] E. Molz, A. P. Y. Wong, M. H. W. Chan, and J. R. Beamish, Phys. Rev. B **48**, 5741 (1993).
[16] C. R. M. Wronski, Br. J. Appl. Phys. **18**, 1731 (1967).
[17] C. J. Coombes, J. Phys. F: Met. Phys. **2**, 441 (1972).
[18] R. Kofman, P. Cheyssac, A. Aouaj, Y. Lereah, G. Deutscher, T. Ben-David, J. M. Penisson, and A. Bourret, Surf. Sci. **303**, 231 (1994).
[19] J. Frenkel, *The Kinetic Theory of Liquids* (Dover, New York, 1956), p. 324.
[20] J. Q. Broughton and G. H. Gilmer, Acta Metall. **31**, 845 (1983).
[21] T. Bachels, H.-J. Güntherodt, and R. Schäfer, Phys. Rev. Lett. **85**, 1250 (2000).
[22] C. E. Bottani, A. Li Bassi, A. Stella, P. Cheyssac, and R. Kofman, Europhys. Lett. **56**, 386 (2001).
[23] S. L. Lai, J. Y. Guo, V. Petrova, G. Ramanath, and L. H. Allen, Phys. Rev. Lett. **77**, 99 (1996).
[24] B. Pluis, D. Frenkel, and J. F. Vanderveen, Surf. Sci. **239**, 282 (1990).
[25] G. L. Allen, R. A. Bayles, W. W. Gile, and W. A. Jesser, Thin Solid Films **144**, 297 (1986).
[26] H. K. Christenson, J. Phys.: Condens. Matter **13**, R95 (2001).
[27] J. M. Titman, Phys. Lett., C **33**, 1 (1977).
[28] E. M. Dickson, Phys. Rev. **184**, 294 (1969).
[29] W. D. Knight and A. G. Berger, Ann. Phys. **8**, 173 (1959).
[30] C. P. Slichter, Philos. Mag. B **79**, 1253 (1999).
[31] E. L. Nagaev, Phys. Rep. **222**, 199 (1992).
[32] J. J. van der Klink and H. B. Brom, Prog. Nucl. Magn. Reson. Spectrosc. **36**, 89 (2000).
[33] P.-A. Vuissoz, J. P. Ansermet, and A. Wieckowski, Phys. Rev. Lett. **83**, 2457 (1999).
[34] K. Kimura, Phys. Rev. B **42**, 6939 (1990).
[35] M. C. Desjonqueres and D. Spanjaard, *Concepts in Surface Physics* (Springer, Berlin, 1998).
[36] M. J. Williams, P. P. Edwards, and D. P. Tunstall, Faraday Discuss. Chem. Soc. **92**, 199 (1991).
[37] E. V. Charnaya, D. Michel, C. Tien, Yu. A. Kumzerov, and D. Yaskov, J. Phys.: Condens. Matter **32**, 5469 (2003).
[38] B. F. Borisov, E. V. Charnaya, P. G. Plotnikov, W.-D. Hoffmann, D. Michel, Yu. A. Kumzerov, C. Tien, and C.-S. Wur, Phys. Rev. B **58**, 5329 (1998).